ATLAS: Energy Dependence of the Intermodule Widening Correction

Neil McBlane
Supervisors: Stefanie Morgenstern, Martin Aleksa

August 25, 2017

Acknowledgements

I would like to thank Stefanie Morgenstern for her continued and attentive support throughout this project, and Martin Aleksa for his suggestions and advice. I would also like to thank the CERN Summer Student Team for making this experience possible, and the Science & Technology Facilities Council for enabling me to be here. Finally I would like to thank my officemates for keeping me entertained through the slower, less successful days.

1 Introduction

The ATLAS Liquid Argon (LAr) Calorimeter is an Electromagnetic calorimeter, capable of precisely measuring the energy of electrons and photons produced by the decays of LHC collision products. Its barrel is split into 16 modules for construction purposes. When assembling these modules into calorimeter wheels, it was unavoidable that the drift gaps at the module boundaries would end up slightly larger than the other gaps. The weight of the calorimeter led to a compression of these gaps on the bottom (hence we observe a small effect there) and a larger opening on top of the calorimeter. As a result, a small underestimation of energy occurs in each.[1]

The previous LAr intermodule widening correction factors were determined using $Z \rightarrow ee$ events taken with the ATLAS detector in 2015 and 2016 at a center of mass energy of $\sqrt{s} = 13TeV$ ($\mathcal{L} = 36.1fb^{-1}$), processed using ATHENA release 20.7 (rel20.7).[2] This project looked to update the factors using the same dataset processed with ATHENA release 21 (rel21) - the most recent release - and extended to include $J/\psi \rightarrow ee$ events. The key development step was including an investigation of the energy dependence: first proposed in 2011, statistics have been insufficient to explore this fully until now.[3]

Once the factors had been determined, they were validated by applying them to the calculation of the invariant mass of the e^+e^- pairs originating from Z and J/ψ decays. As a closing point, parameterization of the effect that energy has on the correction factors is briefly discussed as a possible next step in updating the correction.

Throughout the project, only the barrel was considered as the end-cap demonstrates no observable intermodule widening effect. It is believed this is due to the different construction of the end-cap: although also split into modules, it demonstrates a much greater resistance to gravitational sagging.

2 Comparing Releases 20.7 and 21

In order to initially justify comparison of the correction factors for each release, the two datasets were compared to ensure their similarity.

2.1 Key Variables

A number of factors are key in determining the correction factors, namely:

- eta - η, the pseudorapidity of each recorded electron.

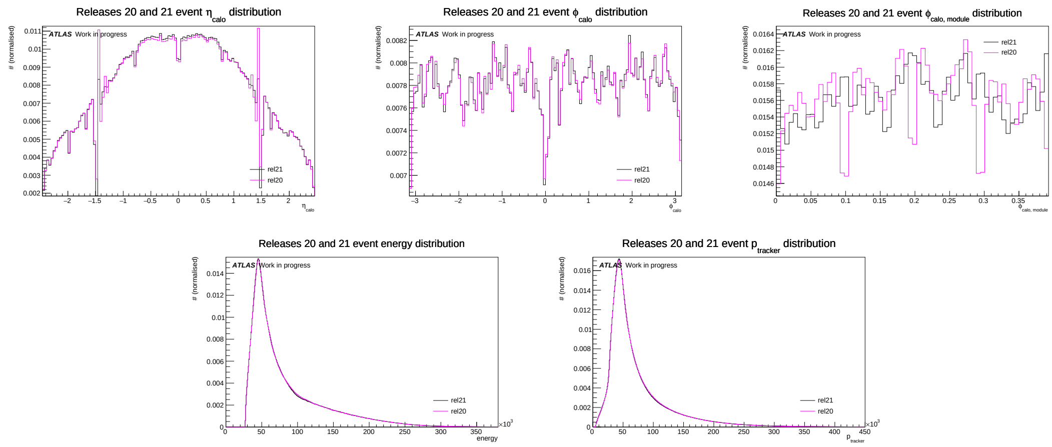

Figure 1: Comparison of the distribution of key variables in release 20.7 and release 21.

- phiCalo - ϕ_{calo}, the azimuthal position of each recorded electron.
- phiCaloModule - $\phi_{calo,module}$, the azimuthal position of each recorded electron within the corresponding LAr Calorimeter module which measured it. An offset of $\pi/32$ is applied to this definition such that the intermodule gap sits at the "center" of each.
- energy - E, the energy of each electron, recorded by the calorimeter.
- pTrack - p_{track}, the momentum of each electron, recorded by the inner detector.

To validate similarity, the distribution of their values for the recorded events was plotted for each release. These can be seen in Figure 1.

There is some variation between the releases, particularly in $\phi_{calo,module}$, but these differences are nominal (e.g. of the order of a percent).

2.2 Intermodule Widening

In Figure 2, E/p_{track} is calculated for each electron then split into 64 bins across $\phi_{calo,module}$ (representative of the finest physical splitting of the detector). Within each of these $\phi_{calo,module}$ bins, a Crystal-Ball fit is made to a histogram of E/p_{track}. The peak and error on the peak are plotted here, with all modules are folded to demonstrate the general effect only.

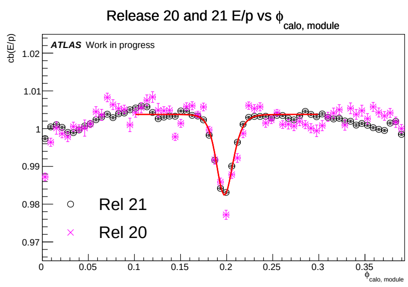

Figure 2: A comparison of the intermodule widening effect in releases 20.7 and 21. A double-Fermi-Dirac fit to release 21 is shown in red.

There are again some fluctuations, but the general shape - particularly around the gap - is similar. Worth noting in both distributions is a general wide curvature which peaks at the gap and is lowest at either end. This may also be due to the geometry of the detector, but is a much smaller effect than the intermodule widening.

2.3 Correction Factor Generality

The rel20.7 correction factors were derived with the electrons split into their individual modules, but inclusive in energy (i.e. a single correction was made for each module for all values of energy).

Thus, for comparison, the first correction factors made from the rel21 data were calculated using the same arrangement of the data. Since we are fitting to a detector intrinsic effect, the corrections derived for the rel20.7 dataset should still correct well for the rel21 dataset, so as a validation step both the rel20.7 and rel21 derived corrections were applied to the rel21 data and, which can be seen for two modules in Figure 3.

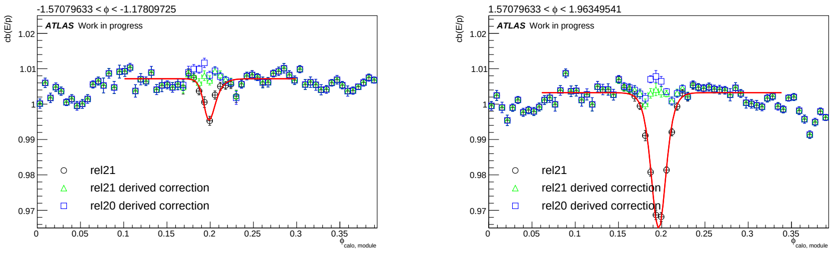

Figure 3: Comparison of the correction factors derived from release 20.7 and release 21 when applied to release 21 data.

The rel21 correction appears to perform better - giving a flatter shape over the gap - but rel20.7 clearly generalizes well, and one could argue that its fluctuation above the gap is in-line with the general curvature of the measurement across $\phi_{calo,module}$. Also demonstrated is the necessity of correcting for each module separately: the factors are vastly different.

3 Improvements to the Correction Factors

As mentioned previously, it was suspected in 2011 that the energy of the electron which enters the intermodule widening gap will have an effect on the size of the detector's underestimation. Figure 4 demonstrates why this was theorized to be the case: shower size scales with energy, so for a small shower a greater fraction of its energy will be lost within the gap, thus a larger underestimation will occur.

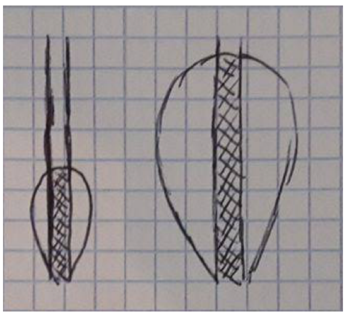

Figure 4: A demonstration of how the fractional underestimation of shower energy scales with shower size and therefore incident electron energy. On the left is a low energy (thus small shower) and on the right is a shower due to a much higher energy electron.

3.1 Derivation from Z Decay Data

In order to study this effect, the rel21 dataset was binned according to the energy of the decay products measured. Bins were chosen by hand to balance the statistics required for fitting with having a sufficient number of bins to observe the effect of changing energy whilst still also splitting in module. Four bins were taken, each with roughly 400,000 electrons contained:

- 0GeV to 39GeV
- 39GeV to 48GeV
- 48GeV to 60GeV
- 60GeV to 500GeV

Figure 5 shows the effect of this binning: we see a clear trend for the size of the correction factor to decrease as the energy increases. As the energy inclusive fit is dominated by events around the Z peak, it overcompensates in the lower bin and under-compensates in the upper. The plots for all modules and energy bins can be found in Appendix A.

Also worth noting is the significant deterioration in the quality of the plot to either side of the dip - it would be difficult to justify decreasing the size of the energy bin further to see more of the relationship using this method.

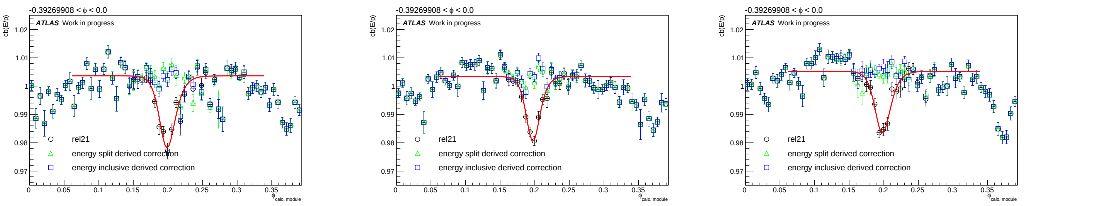

Figure 5: From left to right, 0-39GeV, 39-48Gev and 48-60GeV - each for the same module. The factor for each separate energy bin is plotted in red, with its application compared to that of the energy inclusive correction. There is a clear trend for the correction factor to decrease as energy increases.

If all the modules are folded, the relationship becomes even more clear: Figure 6 shows there appears to be a linear relation between the amplitude of the correction factors and the weighted mean energy of the bin they each correspond to. We believe it to be valid to fold the modules in this way since the effect that energy has on the underestimation should be independent of module. This has the further benefit of significantly increasing the statistics, allowing more bins to be made - something we will explore in more detail later.

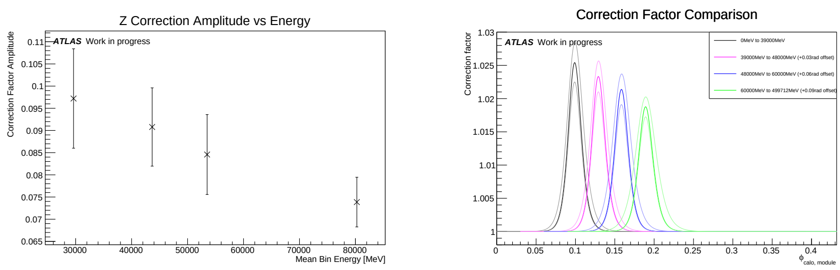

Figure 6: Left: the amplitude of the correction factors as a function of the weighted mean bin energy for the Z decay dominated energy region. The errors are taken directly from the fit. A clear relationship between energy and amplitude is apparent. Right: a plot of the correction factors, with an offset of 0.03 radians applied to each increasing energy factor for visual clarity.

3.2 Application to Z Invariant Mass

The derived correction factors were applied to the energy and momentum values measured for each event within the calorimeter to determine the Z invariant mass, with both the energy split and inclusive methods performing well. Figure 7 summarizes their effect. We see that both corrections increase the measured invariant mass and reduce sigma on this value, as we would expect. we also see a slight reduction in the correction when using the energy split factors, suggesting a slight overcorrection by the inclusive method, but the difference is small.

3.3 Application to J/psi Invariant Mass

The majority of J/ψ events lie within the lowest (0-39GeV) energy bin of the split Z correction. Figure 8 shows that the factors in the bin overcompensate for the intermodule widening gap. To study why this was the case, the J/ψ events were further split into smaller bins, with the modules folded to provide sufficient statistics:

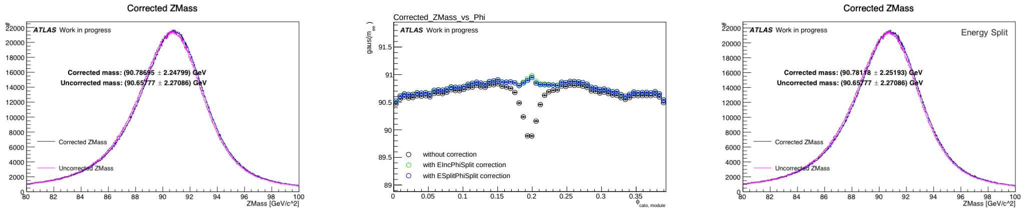

Figure 7: From left to right: the energy inclusive Z mass correction, corrected Z mass distribution vs phi, energy split Z mass correction. The distribution vs phi unfolds the events so that the Z mass for a single boson is plotted at the $\phi_{calo,module}$ position of both the positron and electron from its decay.

- 0GeV to 10GeV
- 10GeV to 20GeV
- 20GeV to 40GeV

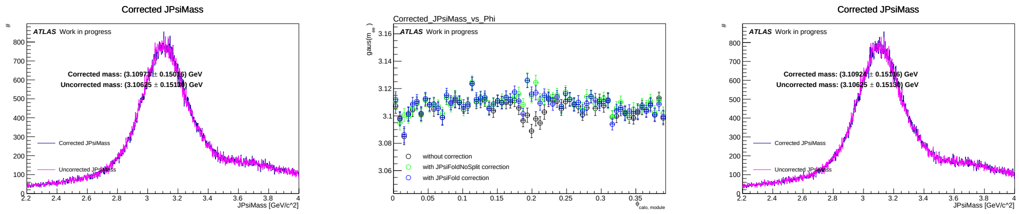

Figure 8: From left to right: the Z derived J/ψ mass correction, corrected J/ψ mass distribution vs phi, Jψ derived J/ψ mass correction. The same unfolding method as for the Z mass is used to plot the invariant mass vs phi. The correction factors derived using the Z decay dominated energy range clearly overcompensates around the gap.

The correction factors from these bins can be seen in Figure 9. There are a few unexpected features here - most notably that the correction amplitude of the lowest energy bin is actually lower than the next bin up. We believe this is due to the significant curvature experienced by low energy electrons under the influence of the magnet in the inner detector leading to a large angle between the shower and intermodule widening gap. As a result, the showers cross the gaps with a larger angle, and the gap widening therefore affects a broader ϕ-window of showers, so the effect is somewhat washed out. This competes against the linearly increasing correction amplitude.

There is a significant increase in the deviation angle of electrons in the inner detector in the energy range 0-10GeV (Fig.10, right), which would point to this being the correct explanation for the drop-off in correction factor amplitude.

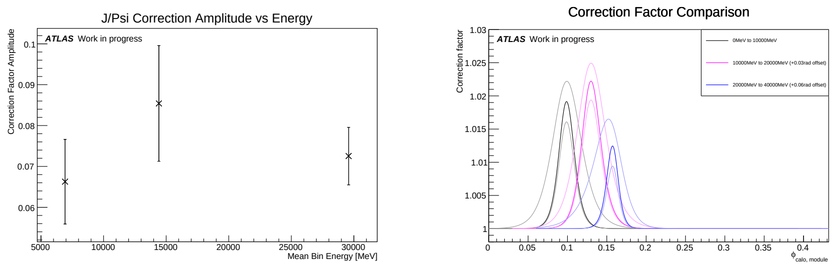

Figure 9: Left: The amplitude of the correction factors as a function of the mean bin energy for the J/ψ decay dominated energy region. The errors are taken directly from the fit. The relationship between amplitude and energy is more complex here than for the Z region - there is competition between electron curvature and shower size, and the 30GeV datapoint is likely spurious due to background. Right: a plot of the correction factors, with an offset of 0.03 radians applied to each increasing energy factor for visual clarity.

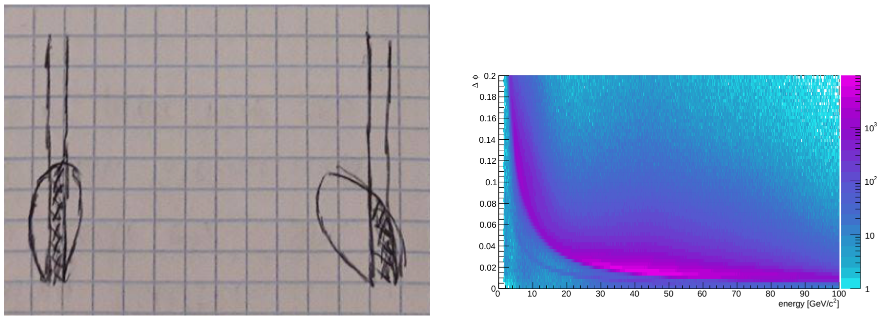

Figure 10: A possible explanation for why the lowest energy correction factors see a reduction in amplitude: showers crossing the gaps with a larger angle present a broader ϕ-window, leading to a blurring out of the intermodule widening effect. The region we see this effect most prominently in is 0-10GeV, and this corresponds to the region of most significant curvature.

We believe the correction factor corresponding to the highest energy bin in J/ψ dominated region to be spurious given it likely only contains background events.

Application of these J/ψ specific correction factors does provide a slight improvement to the invariant mass distribution, but its effect is nominal (Fig.8).

4 Next Steps

Clearly there exists a relationship between energy and correction factor amplitude, with some competition between its effect and the curvature of low energy electrons. If this relationship could be properly parameterized, it would allow for consideration of the effect of energy to be made without having to sacrifice the statistics of the data. Due to the significant statistics made available by folding the data across the modules, it is possible to bin more finely in energy to look at this effect in detail.

Neglecting the low energy entry angle dominated regime (for now - further study should be done on this), if one makes some simplifying assumptions, it is possible to derive (see Appendix B) a relationship between the expected correction factor and energy:

$$cf = \xi \frac{\alpha(\log(E) - 1.987)}{\alpha(\log(E) - 1.987) - \beta} \tag{1}$$

Where α, β and ξ are constants to be determined. Fitting this, and a simplistic linear model, to the more finely binned data (Fig.11) indicates that a parametric compensation is likely a viable solution - though the exact model will need further development, Equ.1 appears to be a vast oversimplification - for instance, it does not take into account the unequal distribution of energy within the shower.

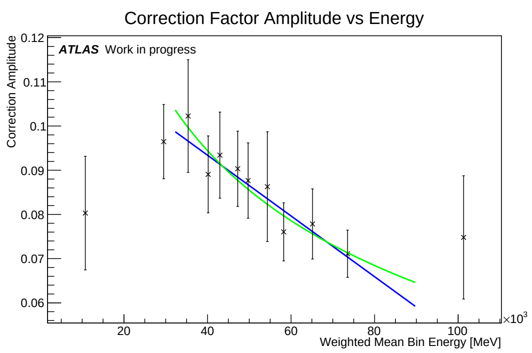

Figure 11: The amplitude of the correction factors as a function of the weighted mean bin energy for the Z decay dominated energy region, folded in module and more finely binned than previously. The green line indicates the fit to Equ.1 and the blue is a simple linear fit.

Appendix A

Dropbox link to all fits: https://www.dropbox.com/sh/29bintpf8o3ba4f/AADFeclfsSc4lrUbZo1VwEYRa?dl=0

Appendix B

To (very) roughly estimate the dependence of the correction factors on energy, one can treat the electron shower as a teardrop shape whose volume is consists of a hemisphere and a cone. Assuming a constant relationship between radius and longitudinal length (i.e. for the cone, $h = \gamma r$), the volume is thus:

$$V_T(r) = V_H(r) + V_C(r,h) = \frac{2}{3}\pi r^3 + \frac{\gamma}{3}\pi r^3 = \alpha r^3 \tag{2}$$

We then assume the intermodule widening gap to be a cuboid whose volume contained within the teardrop is proportional to its radius and longitudinal length:

$$V_G(r,h) = \tau r h = \beta r^2 \tag{3}$$

Thus the fractional volume loss is given by:

$$f = \frac{V_T(r) - V_G(r)}{V_T(r)} = \frac{\alpha r - \beta}{\alpha r} \tag{4}$$

Where α and β are constants to be determined. Using the usual shower depth approximation:

$$X = X_0 \frac{\log(E_0/E_c)}{\log(2)} \propto \log(E) - \log(7.3) = \log(E) - 1.987 \tag{5}$$

Where X_0 is the radiation length of the material (lead for the LAr calorimeter), E_c is the critical energy (approximately 7.3MeV for electrons in lead [4]) and E_0 is the energy of the incident electrons.

Since we have assumed that the longitudinal length and radius are proportional, we can then absorb any proportionality into α, giving:

$$f = \frac{\alpha(\log(E) - 1.987) - \beta}{\alpha(\log(E) - 1.987)} \tag{6}$$

Assuming an inverse relationship between the correction factor and fractional volume contained within the gap, we therefore have:

$$cf = \xi \frac{\alpha(\log(E) - 1.987)}{\alpha(\log(E) - 1.987) - \beta} \tag{7}$$

References

[1] ATLAS Collaboration, *The ATLAS Experiment at the CERN Large Hadron Collider*, JINST 3 (2008) S08003.

[2] ATLAS Collaboration, *ATL-COM-PHYS-2017-758*, Available at: https://cds.cern.ch/record/2268802?ln=en

[3] ATLAS Collaboration, *ATL-COM-PHYS-2013-1421*, Available at: https://cds.cern.ch/record/1608607?ln=en

[4] pdg.lbl.gov (2015). *Atomic and nuclear properties of lead (Pb)* [online] Available at: http://pdg.lbl.gov/2015/AtomicNuclearProperties/HTML/lead_Pb.html [Accessed 25 Aug. 2017].